An Adaptive Richardson-Lucy Algorithm for Medical Image Restoration

Qunoot A. Yaqoub and Ayad A. Al-Ani

College of Information Engineering, Al-Nahrain University, Baghdad, Iraq

https://doi.org/10.26636/jtit.2023.168222

Abstract — Image restoration is the process of estimating the original image content from a degraded picture. In this paper, the Richardson-Lucy iterative algorithm was developed to improve the quality of degraded medical images. It has been assumed that medical images are exposed to two types of degradation. The first type is the blur function in the Gaussian form with different widths, i.e. σ = 1, 2, and 3. The second type of degradation was assumed to be of the independent white Gaussian noise type with different signal-to-noise ratio values: SNR = 10, 50, and 100. The results obtained from the adaptive filter are compared, quantitatively, with different conventional filters: inverse, Wiener, and constraint least square, by applying different measures, such as: power signal to noise ratio (PSNR), structural similarity index (SSID), and root mean square error (RMSE). The comparison showed that the adaptive recovery filter achieves better results.

Keywords — constraint least square filter, Gaussian blurring function, Gaussian noise function, inverse filter, non-blind deconvolution, point spread function, Richardson-Lucy algorithm, Wiener filter.

1. Introduction

In many applications, recorded or generated images are a degraded version of the original picture due to flaws in the imaging and capturing processes. These imperfections are very difficult to remove. The process of eliminating them is, therefore, an important task in image processing [1]. Flaws or degradation may be caused by noise or may result from blurring. Blurring can occur during image creation, transmission, and storage, and may result from transmission channel error, camera defects, atmospheric turbulence, relative motion between the object and the camera, as well as other factors [2]. The term “noise” refers to an unwanted random variation in brightness that affects the image. Such noise is part of the ideal signal and can be caused by a variety of factors, such as poor detector sensitivity, environmental factors, the discrete nature of radiation, transmission or quantization errors, and so on [3]. Additive noise and multiplicative noise are the two types of interference encountered. Additive noise is a linear image additive that is unaffected by the strength of the input signal. The Gaussian distribution with a mean of zero is used to represent the probability density function. Noise is also assumed to be white because its spectrum power distribution is nearly constant. Multiplicative noise differs depending on whether the input signal is multiplicative or correlated with the original signal. The Poisson distribution is used to represent this type of noise [4]. The relationship between a degraded (blurry and noisy) image $g(x, y)$ and the object (original image) $f(x, y)$ is given by [1]:

$$g(x, y) = h(x, y) \otimes f(x, y) + n(x, y)\,, \tag{1}$$

where $n(x, y)$ is the additive white Gaussian noise, $h(x, y)$ is the blurring function, also known as the point spread function (PSF), and $\otimes$ denotes the convolution process.

Medical imaging is nowadays essential for guiding disease diagnosis and treatment. One of the most basic and crucial aspects of medical imaging is image reconstruction. The main goal is to have high-quality clinical images used at the lowest possible cost and risk to the patients. Medical imaging devices may aid in early detection of diseases and, thus, in improving public health. MRI and CT scans, for example, are degraded by poor quality of equipment or patient movements during the image acquisition phase. This results in images that are mostly unusable. This shows that medical images must be of high quality to offer a quick and accurate diagnosis. To remove blurring and noise from degraded images, restoration processes must be performed. The goal of the restoration process is to estimate an image that is as close as possible to the original image $f(x, y)$, based on its degraded counterpart $g(x, y)$ [5]. There are two types of image deconvolution algorithms: blind (in which both PSF and noise are unknown) and non-blind (in which both PSF and noise are known). The blurring PSF and SNR from noise added are not known ahead of time in the case of blind restoration [6]. Figure 1 shows the degradation and restoration phases.

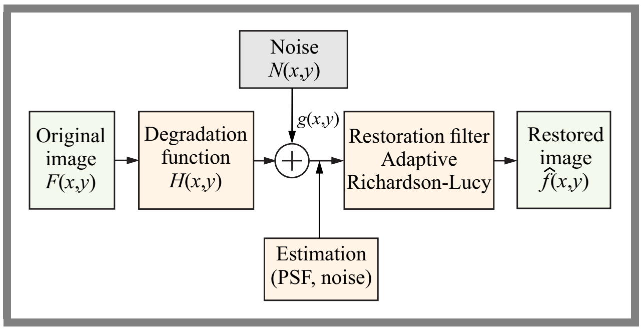

Fig. 1. Image degradation and restoration phases.

In this study, an iterative restoration technique known as the Richardson-Lucy algorithm (R-L) was adopted. A modified filter was created to restore CT scan medical images that have been blurred with a Gaussian function in different standard deviation (STD) "width" of PSF = 1 and 3, and also corrupted by adding white Gaussian noise with different degrees of noise variance, i.e. with SNR = 10, 50, and 100.

The R-L algorithm has a problem with amplified noise and introduces the ringing effect as the number of iterations is increased, which also renders the computational process complex. The current research concept is based on the enhancement of the R-L algorithm in order to investigate the effect of strengthening the image's edges during the restoration process, as well as the ability of the proposed algorithm to eliminate ringing and noise issues. This is accomplished by introducing two parameters, λ and β, into the equation with varying values, as well as calculating image edge detection parameters using the Sobel edge detection approach. Then, we compare the outcomes using various restoration filters, including inverse, Wiener, constraint least squares filter (CLSF), and the standard R-L, before modifying the image, in order to investigate how this development could affect the outcomes of the image restoration process. The effectiveness of this approach is determined using specific criteria, including mean square error (MSE), peak signal to noise ratio (PSNR), and structural similarity index (SSIM).

The main contributions of this study are:

- to represent the effect of adding to the priory restored image $f^{(k)}(x, y)$ with some β weight,
- to strengthen the image's edges, adding the edges to the priory restored image with some λ weight.

The rest of this document is organized as follows. Section 2 offers an review of existing approaches that may be found in the literature. Section 3 describes the general recommended framework. Section 4 assesses our research experiment. Section 5 concludes the paper.

2. Related Works

Many research models focusing on this topic have been implemented to date. However, each strategy employed was tailored to a specific application area. Panfilova *et al.* [7] proposed a method of restoration consisting in extending the image beyond its original borders, reducing its brightness to zero at the new borders, and using an empirical criterion for defining the point at which the iterative process ends. To lessen the negative impact of the image restoration problem, linear blur compensation is applied. The Richardson-Lucy iterative method and its modifications are used to restore the image. The proposed modifications reduced image distortion by more than 50% in terms of the RMS metric, allowing the authors to estimate the number of iterations required to ensure better performance of the algorithm.

Anacona-Mosquera *et al.* [8] presented hardware for implementing the R-L algorithm and for accomplishing the image restoration task, where the images are blurred due to the camera's motion relative to the scene. The R-L was implemented in this case with the use of an FPGA-based platform relying on VHDL and with assumption that the capturing image system is free of additive noise. The overall architecture scales from 3×3 to 9×9 mask sizes for the R-L convolution steps. The high digital signal processing complexity of this architecture, which depends on the number of iterations to be implemented, is a disadvantage.

Tselousov *et al.* [9] proposed a hybrid estimation method based on cepstral and gradient field analysis of the distorted image. The method offers better performance in terms of blind deconvolution image restoration based on the Bayes approach. The Richardson-Lucy engine revealed that, in most cases, images distorted by camera shake are characterized by better visual quality.

Aouinti *et al.* [10] introduced a genetic approach to optimize the iteration count of the R-L deconvolution to obtain a better restoration of degraded satellite images, enhancing image quality by increasing SNR. Panfilova *et al.* [11] proposed a control algorithm for R-L restoration to end its iterative procedure based on the criteria defined by the quality measure introduced. It was discovered that the restoration quality criteria based on the analysis of inter-line and inter-column correlation coefficients act as an alternative rather than a subordinate to other quality measures in use.

Liu *et al.* [12] improved the performance of the star sensor network working in a highly dynamic environment, using the R-L algorithm based on a radial basis function neural network (RBFNN). Firstly, using angular velocity information provided by a gyroscope, the point spread function (PSF) is calculated. RBFNN is then used to predict how many iterations the R-L algorithm will require to complete the process of deblurring the star image. The authors demonstrated that quality of the deblurred star image is excellent, even at high angular rates. Breykina *et al.* [13] developed an algorithm for automated image restoration based on the analysis of line-to-line and column-to-column correlation coefficients. The R-L method is used for image reconstruction in order to refine the distortion operator iteratively, and gradient descent is used to estimate the distorting operator. Experiments showed that images with smear and blur distortion yield correct restoration results, and that the method reduces the number of calculations required.

Zhao *et al.* [14] proposed a new image quality assessment index-based on the R-L algorithm. This method was designed for self-adaptive image de-blurring. Through experimental verification and comparison to other methods, the authors prove that the method achieves higher levels of efficiency, accuracy, and real-time performance. Bhonsle proposed, in [15], the R-L algorithm to correct the blurring problem, and the krill herd optimization to fine-tune the quality of the restored image, which results in a better restored image with higher PSNR, SNR and SSIM metrics.

Lyu *et al.* [16] attempted to improve ultrasonic c-scan image quality by combining the R-L algorithm and a faulty measurement model. Through the restoration of the simulated images, a connection between the optimal number of iterations and the flaw size-to-sound wavelength ratio is established, and the R-L iterative algorithm is used to restore the experimental ultrasonic c-scan images with the optimal number of iterations. The proposed restoration method improves the accuracy of ultrasonic c-scan imaging significantly.

Li *et al.* [17] presented the Richardson-Lucy network (RLN), a fast and lightweight deep learning method for the deconvolution of three-dimensional fluorescence microscopy. The R-L is combined with a fully convolutional network structure in RLN, establishing a connection to the image formation process and thus improving network performance. The authors prove that RLN outperforms classical R-L deconvolution on volumes contaminated with severe out-of-focus fluorescence or noise, and it reconstructs large, cleared-tissue datasets four to six times faster than traditional multi-view pipelines.

3. Proposed Method

The purpose of this paper is to recover the quality of degraded medical images by using an inverse filter, Wiener filter, constrained least squares filter (CLSF), and the Richardson-Lucy algorithm to restore original images and to compare these results with adaptive Richardson-Lucy filter. Figure 2 shows the architecture of the proposed system.

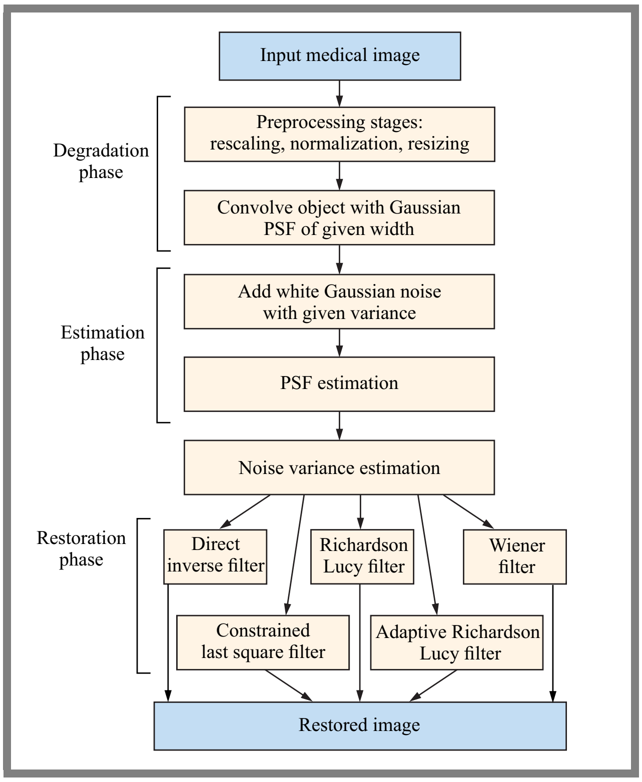
Input medical image
Degradation phase
Preprocessing stages: rescaling, normalization, resizing
Convolve object with Gaussian PSF of given width
Estimation phase
Add white Gaussian noise with given variance
PSF estimation
Noise variance estimation
Restoration phase
Direct inverse filter
Richardson Lucy filter
Wiener filter
Constrained last square filter
Adaptive Richardson Lucy filter
Restored image

Fig. 2. Block diagram of the proposed system.

Direct inverse filtering is the simplest method of restoration. In this method, the Fourier transform (FT) of the degraded image $G(u,v)$ is divided by the FT of the degradation function $H(u,v)$ to estimate of the FT of the image $F(u,v)$ [18]:

$$F(u,v) = \frac{G(u,v)}{H(u,v)} \, . \tag{2}$$

This method works fine when the degraded image contains no additive noise. The inverse filter has the advantage of requiring only the blur PSF as a priori knowledge and allowing for perfect restoration in the absence of noise. As a result, it excessively dominates inverse-filtered images.

The Wiener filter is also known as the minimum mean square estimator. Some of the difficulties associated with inverse filtering were alleviated by attempting to recreate the error in the restored image using statistical methods. After modeling the error mathematically, the average error is minimized. As a result, the term minimum refers to a square estimator. The Wiener filter equation is [4]:

$$F(u,v) = \frac{H^*(u,v)}{|H(u,v)|^2 + \frac{\delta_n(u,v)}{\delta_f(u,v)}} G(u,v) \, , \tag{3}$$

where $H^*(u,v)$ denotes the complex conjugate of $H(u,v)$, $\delta_n(u,v)$ is the noise power spectrum, and $\delta_f(u,v)$ is the original image power spectrum.

The constrained least squares filter (CLSF) is another method for overcoming some of the Wiener filter's drawbacks, because only prior knowledge of the noise's mean and variance is required. This is accomplished by incorporating a smoothing criterion into the filter derivation, so that the result does not contain undesirable oscillations which affect the image by forming "waves". The constrained least squares filter is given by [8]:

$$F(u,v) = \frac{1}{H(u,v)} \left| \frac{|H^*(u,v)|^2}{|H(u,v)|^2 + \gamma |p(u,v)|^2} \right| G(u,v) \, , \tag{4}$$

where γ is the adjustment factor, $p(u,v)$ is the smoothness criterion's Fourier transform (FT). The value is determined experimentally and is application dependent. A common function to use for $p(x,y)$ which is the inverse Fourier transform of $P(u,v)$ is the mask of the Laplacian filter [4]:

$$P(u,v) = \begin{vmatrix} 0 & -1 & 0 \\ -1 & 4 & -1 \\ 0 & -1 & 0 \end{vmatrix} \, , \tag{5}$$

3.1. Richardson-Lucy Deconvolution

The Richardson-Lucy deconvolution is a well-known image restoration method classified as a non-blind image restoration approach, because it necessitates prior knowledge of the blur and noise [13]. It is an iterative process that is dependent on the number of iterations, i.e. the most important factor in determining image quality. The R-L algorithm can be used efficiently when PSF is known or there is little or no noise data available [19]. The R-L algorithm is built on a maximum likelihood technique which uses Poisson statistics to model the image. Maximizing the model's likelihood function produces an equation that is satisfied when the next iteration converges [15]. The R-L algorithm was derived from Bayes' theorem. Because it is based on conditional probabilities, the algorithm considers statistical fluctuations in the signal and can thus reconstruct degraded images. Bayes' theorem is given by [20]:

$$p(x|y) \frac{p(y|x)p(x)}{\int p(y|x)p(x) \mathrm{d}x} \, , \tag{6}$$

where $p(y|x)$ is the event's conditional probability y, given event x. $p(x)$ is the probability of event x, and $p(x|y)$ is the conditional probability in reverse, i.e. the probability of event x given event y. Probability $p(x)$ can be identified as the distribution of objects $f(x)$, while conditional probability $p(y|x)$ can be recognized as PSF-centered at x, i.e., $g(y, x)$. Probability $p(y)$ can be recognized as a degraded image or a convolution $c(y)$. The Richardson-Lucy algorithm equation is defined as [21]:

$$f^{(k+1)}(x,y) = \left[\frac{g(x,y)}{h(x,y) \otimes f^{(k)}(x,y)} \otimes h^T(x,y)\right] f^{(k)}(x,y) \ , \quad (7)$$

where $f^{(k+1)}(x, y)$ is the new estimate of a blurred image from the previous one $f_{(i)}(x, y)$, $g(x, y)$, i is the iteration step, $h(x, y)$ is the blur filter (PSF) and $h^T(x, y)$ is the complex conjugate of PSF h, while $\otimes$ denotes convolution.

The R-L deconvolution algorithm has gained popularity in astronomy and medical imaging [20]. It is one of the most widely used deblurring algorithms in the field of image processing. It happens for a variety of reasons, including the fact that it operates efficiently regardless of the type of noise affecting the image. Furthermore, it does not require any information from the original clean image. This algorithm works in the presence of noise, but the noise increases along with the increase in the number of iterations [21]. Despite its benefits, the R-L method has several serious drawbacks, e.g. noise amplification.

3.2. Sobel Edge Detection

In an image, an edge is formed between the boundaries of two distinct regions [22]. The main goal of edge detection is to reduce the amount of data that needs to be processed by simplifying the pixels that make up the image's boundaries. The Sobel edge detection filter is one of the best edge detection algorithms, with a relatively low complexity [23]. The algorithm recognizes the boundaries of an image's horizontal and vertical axes separately. Typically, a pair of 3×3 horizontal and vertical convolution kernels is used by the Sobel operator to perform a 2D spatial gradient measurement on images [24]. To calculate approximate derivatives, the Sobel operator is given by two kernels (G_x, G_y) that are convolved with the original image. One of the kernels is for horizontal changes, and the other one is for vertical modifications, and at each location in the image, it can be written as [24]:

$$G = \sqrt{G_x^2 + G_y^2} \ . \quad (8)$$

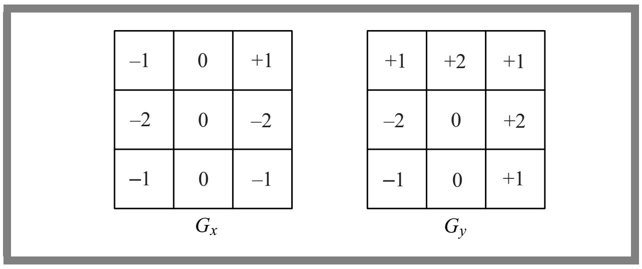

–1	0	+1
–2	0	–2
–1	0	–1

G_x

+1	+2	+1
–2	0	+2
–1	0	+1

G_y

Fig. 3. Sobel masks with 3×3 dimensions.

As shown in Fig. 2, the first kernel G_x determines the incline in the x (columns) direction, while the other kernel G_y determines the tilt in the y (rows) direction [23].

4. Experimental Results and Discussions

The proposed work was implemented using the Matlab software. Before the restoration process, different preprocessing steps of raw data are completed.

Rescaling – the input image must be changed from an RGB color image to a 8-bit grayscale space picture in order to reduce the amount of data needed to represent the image. Consequently, computational efficiency and speed will be increased significantly. The conversion is given by a common formula from [25]:

$$\text{Gray} = 0.30 \text{ R} + 0.59 \text{ G} + 0.11 \text{ B} \ . \quad (9)$$

Normalization – the process of data normalization makes sure that every input parameter has a consistent data distribution for each pixel. As a result, data is normalized by subtracting the mean from each pixel and dividing the result by the standard deviation (STD) value. The normalization process can be expressed as [26]:

$$x_{new} = a + \frac{(x - m_{\min})(b - a)}{(x_{\max} - x_{\min})} \ , \quad (10)$$

where x represents a collection of the observed values, $x_{\min}$ represents the minimum values and $x_{\max}$ represents the maximum values in entire collection.

Resizing an image increases or decreases its resolution and is equivalent to scaling. The image size can be specified manually or by using a scaling factor. There are various algorithms for resizing an image that is stored in a compressed form, e.g. [27] which converts an image of size $m \times m$ into an image of size $k \times k$, where m is the number of pixels in the original image and k is the number of pixels in the compressed image.

4.1. Degradation Phase

A blurred image is produced by convolving the original image with Gaussian PSF. Two different values of PSF widths have been taken in consideration: $\sigma = 1$ and 3, as shown in Fig. 4b-c. To simulate a noisy image, we add white Gaussian noise (WGN) to the original one to achieve SNR = 10, 50, and 100, as shown in Fig. 4d-i.

4.2. Estimation Phase

In the case of blind restoration, the degradation parameters (PSF, noise) must be estimated. Inverse, Wiener, constraint least squares (CLSF) and R-L filters are non-blind restoration techniques. Known degradation parameters are applied to the degraded image during processing. Therefore, PSF and

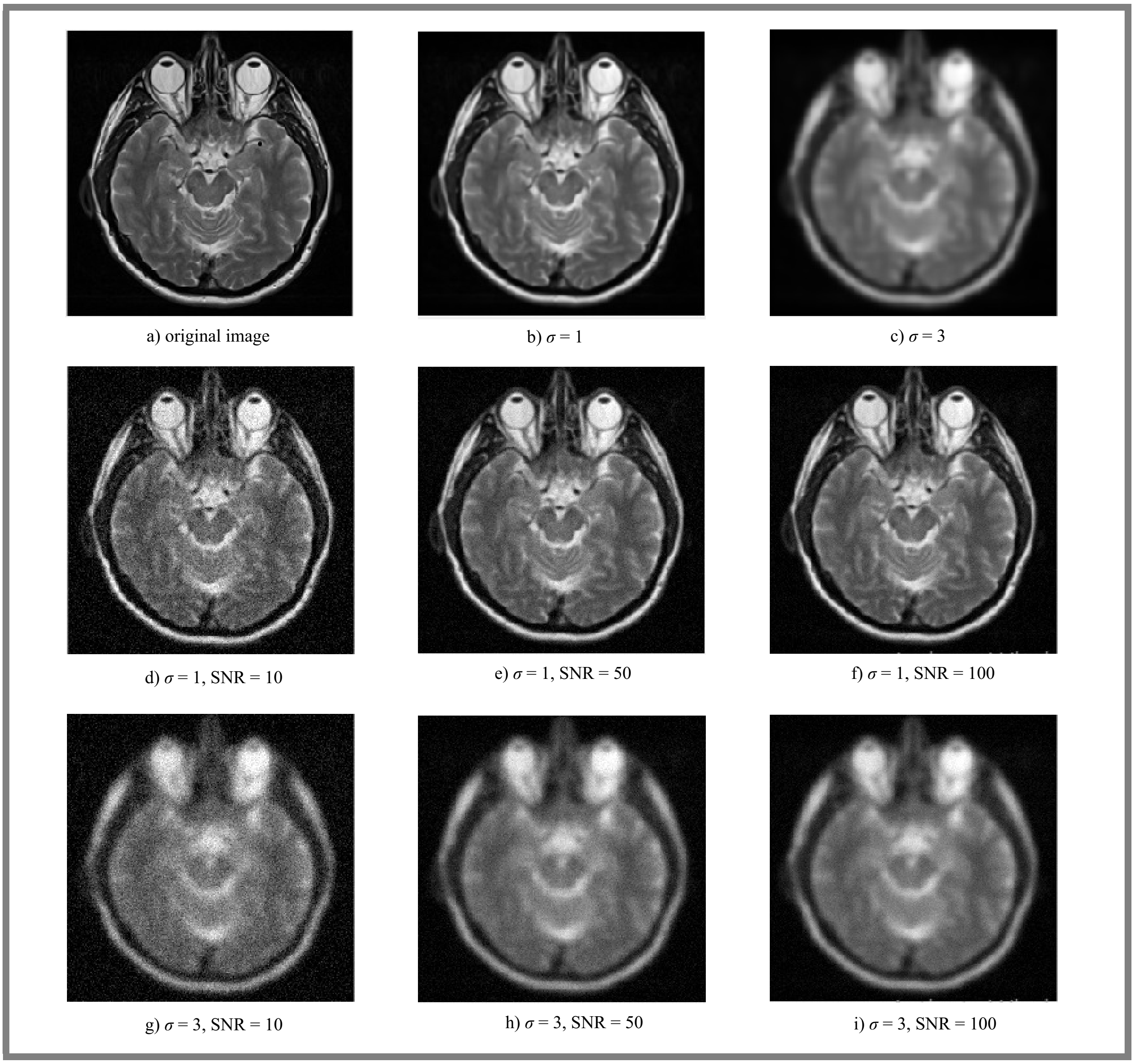
a) original image
b) $\sigma = 1$
c) $\sigma = 3$
d) $\sigma = 1$, SNR = 10
e) $\sigma = 1$, SNR = 50
f) $\sigma = 1$, SNR = 100
g) $\sigma = 3$, SNR = 10
h) $\sigma = 3$, SNR = 50
i) $\sigma = 3$, SNR = 100

Fig. 4. Results of a degraded CT scan image for different values of σ and SNR.

noise must be estimated by using one of the estimations techniques.

4.3. Restoration Phase

To restore the original image $f(x, y)$, filters such as the inverse filter, Wiener filter, constraint least squares filter (CLSF) and R-L have been used. All filters were used to restore the degraded CT scan image, blurred with the Gaussian blurring function with various standard deviation values and distorted with Gaussian noise with different noise levels.

We note from Fig. 5, which represents the effect of a restored CT scan image for different values of σ and SNR by using the inverse filter, that the restored images are not good and the landmarks and details are not clear with or without noise and different values of PSF.

From Fig. 6, which represents the effect of a restored CT scan image for different σ and SNR values by using the Wiener filter, we note that the restored images look good for small PSF levels in the absence of noise, but quality is bad when the noise is present and PSF is increased.

From Fig. 7, which represents the effect of restoration by using CLSF, we see that the restored images are good for low PSF values in the absence of noise, but with high PSF levels, the resonance effect begins to appear on the edges. Moreover, when the noise is present, the image quality decreases with high PSF and low SNR.

4.4. Adaptive Richardson-Lucy Filter

Development of an RL algorithm to eliminate the problem of noise amplification and reduce the number of iterations

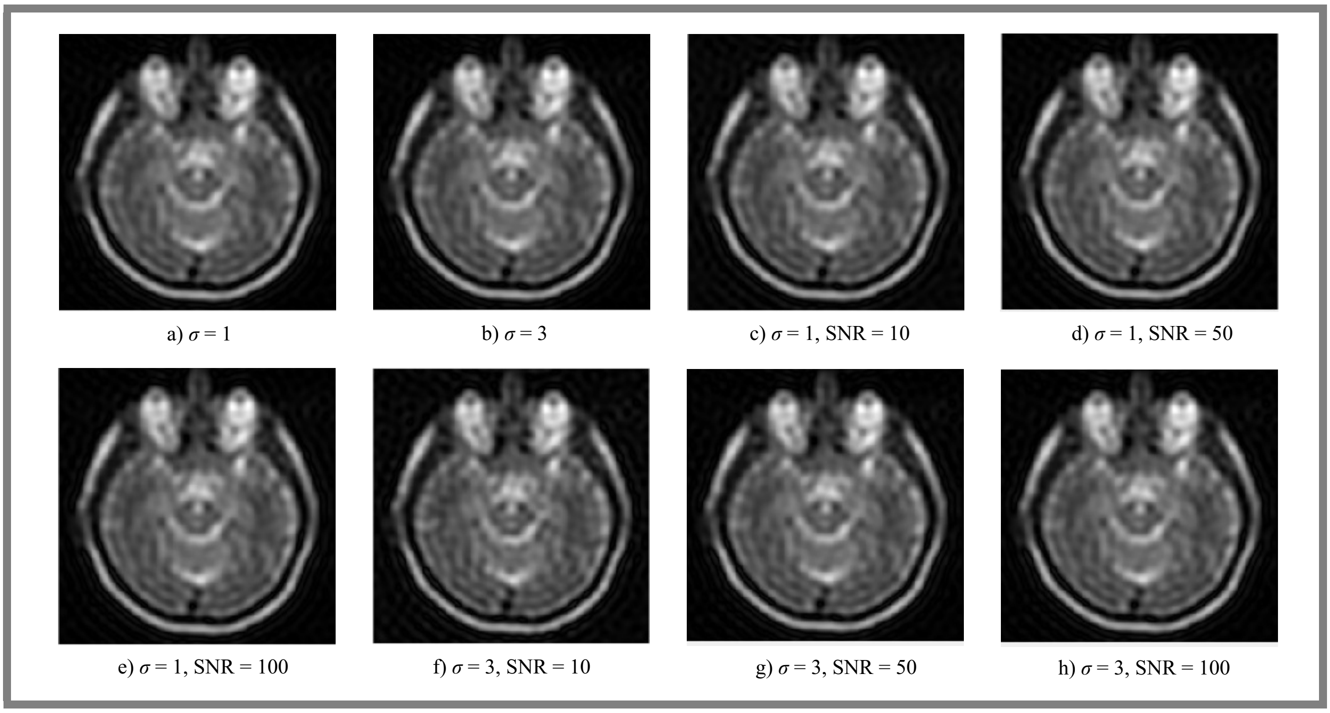

a) $\sigma = 1$ b) $\sigma = 3$ c) $\sigma = 1$, SNR = 10 d) $\sigma = 1$, SNR = 50

e) $\sigma = 1$, SNR = 100 f) $\sigma = 3$, SNR = 10 g) $\sigma = 3$, SNR = 50 h) $\sigma = 3$, SNR = 100

Fig. 5. Results of restoration for different σ and SNR values by using the inverse filter.

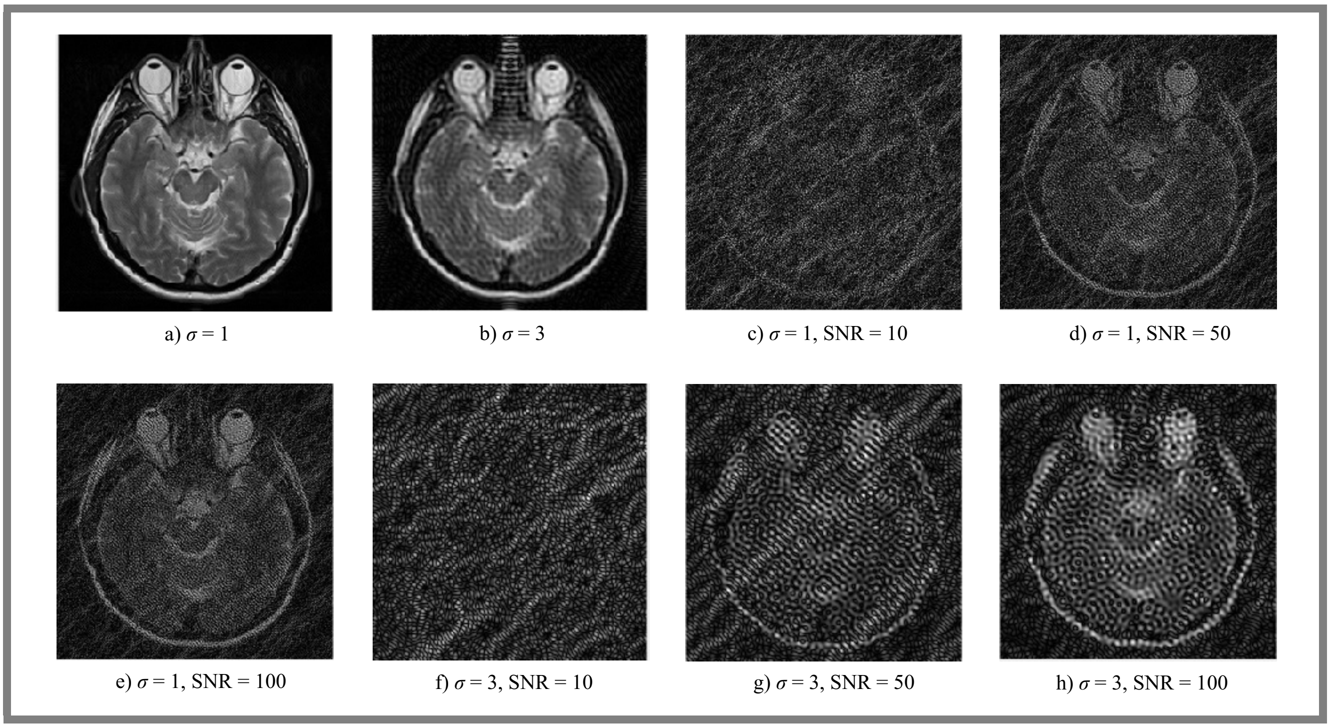

a) $\sigma = 1$ b) $\sigma = 3$ c) $\sigma = 1$, SNR = 10 d) $\sigma = 1$, SNR = 50

e) $\sigma = 1$, SNR = 100 f) $\sigma = 3$, SNR = 10 g) $\sigma = 3$, SNR = 50 h) $\sigma = 3$, SNR = 100

Fig. 6. Results of image restoration for different σ and SNR values using the Wiener filter.

since the increasing iteration causes increase the effect of resonance on the image. In our research, two new adaptations have been introduced. These two adaptations are done by introducing two parameters into the original RL algorithm:

- the first additive term represents the priori restored image (restored image from the previous iteration), through the iteration process of specified weighting factor β, in order to reduce the number of iterations,
- second additive term represents the strengthing of the edges of the images, during the restoration process of the specified weighting factor λ.

The final RL filter after adding the above two new parameters can be described as:

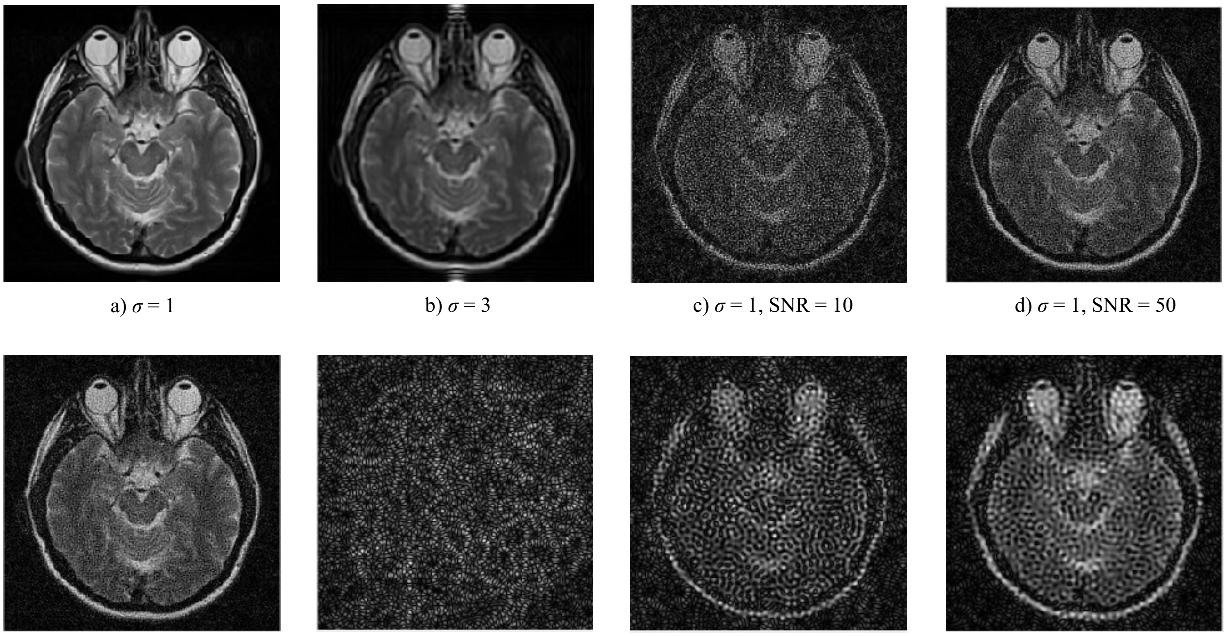

a) σ = 1

b) σ = 3

c) σ = 1, SNR = 10

d) σ = 1, SNR = 50

e) σ = 1, SNR = 100

f) σ = 3, SNR = 10

g) σ = 3, SNR = 50

h) σ = 3, SNR = 100

Fig. 7. Results of restoration of a CT scan image for different σ and SNR values by using the CLSF.

$$\widehat{f}_{(i+1)}(x,y) = \left[\frac{g(x,y)}{h(x,y)\otimes f_{(i)}(x,y)} \otimes h^T(x,y)\right] f_{(i)}(x,y) + \beta f_{(i)}(x,y) + \lambda\big(f_{(i)}(x,y)\otimes s(x,y)\big) \quad (11)$$

where $s(x,y)$ represents the Sobel operator.

Algorithm 1 shows the steps of the restoration filter by using an adaptive RL filter.

Algorithm 1. Adaptive Richardson-Lucy filter.

Input: degraded image, estimated point spread function (PSF), number of iteration (I).

Output: restored image $\widehat{f}_{(i+1)}(x,y)$

```
1: Set value of $f_{(i)}(x,y) = g(x,y)$ in the first iteration
2: Calculate the transpose of matrix $h^t(x,y)$
3: Choose $\gamma$ and $\beta$ within the range 0 to 1 with an increment of 0.25
4: For $i = 1, 2, 3, \ldots, I$
5: Convolve the estimation PSF $h(x,y)$ with the previous estimate value of $f_{(i)}(x,y)$ to produce a reblurred image:
       $h(x,y) \otimes f_{(i)}(x,y)$
6: Divide the blurred image $g(x,y)$ by the value from step 5
7: Convolve the value from step 6 with transpose of matrix $h^t(x,y)$
8: Multiply the value from step 7 with the previous estimated value of $f_{(i)}(x,y)$
9: Multiply $\beta$ with the previous estimated value of $f_{(i)}(x,y)$:
       $\beta f_{(i)}(x,y)$
10: Add the value from step 8 to the value from step 9
11: Apply Sobel edge detection to the previous estimated value of $f_{(i)}(x,y)$:
       $f_{(i)}(x,y) \otimes s(x,y)$
12: Multiply $\lambda$ with the value from step 11
13: Add the value from step 10 to the value from step 12 to $\widehat{f}_{(i+1)}(x,y)$ calculate the new estimate of restored image
14: Repeat until iteration $>$ maximum
15: Return $\widehat{f}_{(i+1)}(x,y)$
```

Figure 8 represents the effect of a restored CT scan image for different λ and β values using various filters in the following order: a) non-blurred, b) Gaussian blurred with σ = 3, SNR = 10, c) restored by inverse filter, d) restored by Wiener filter, e) restored by CLSF, f) restored using R-L method, g) restored using R-L λ = 0.5, h) restored using modified R-L method; λ = 0.5, β = 0.25, and i) restored using modified R-L method, λ = 0.25, β = 1.

4.5. Performance Evaluation

To demonstrate and evaluate the performance of the image restoration and enhancement techniques, several metrics have been used. First, we simulate the degraded images with different cases, i.e. Gaussian for blurring, different degrees of blurring, and different standard deviation "widths" of PSF, σ = 1, and 3, and so on. We also added white Gaussian noise of varying intensities to the noise function, i.e. different degrees of noise variance, different SNR = 5, 10, and 100. Figure 5 shows the original and degraded image using various degradation parameters.

Three different metrics have been used to validate the degree of similarity and loss of quality between the original image

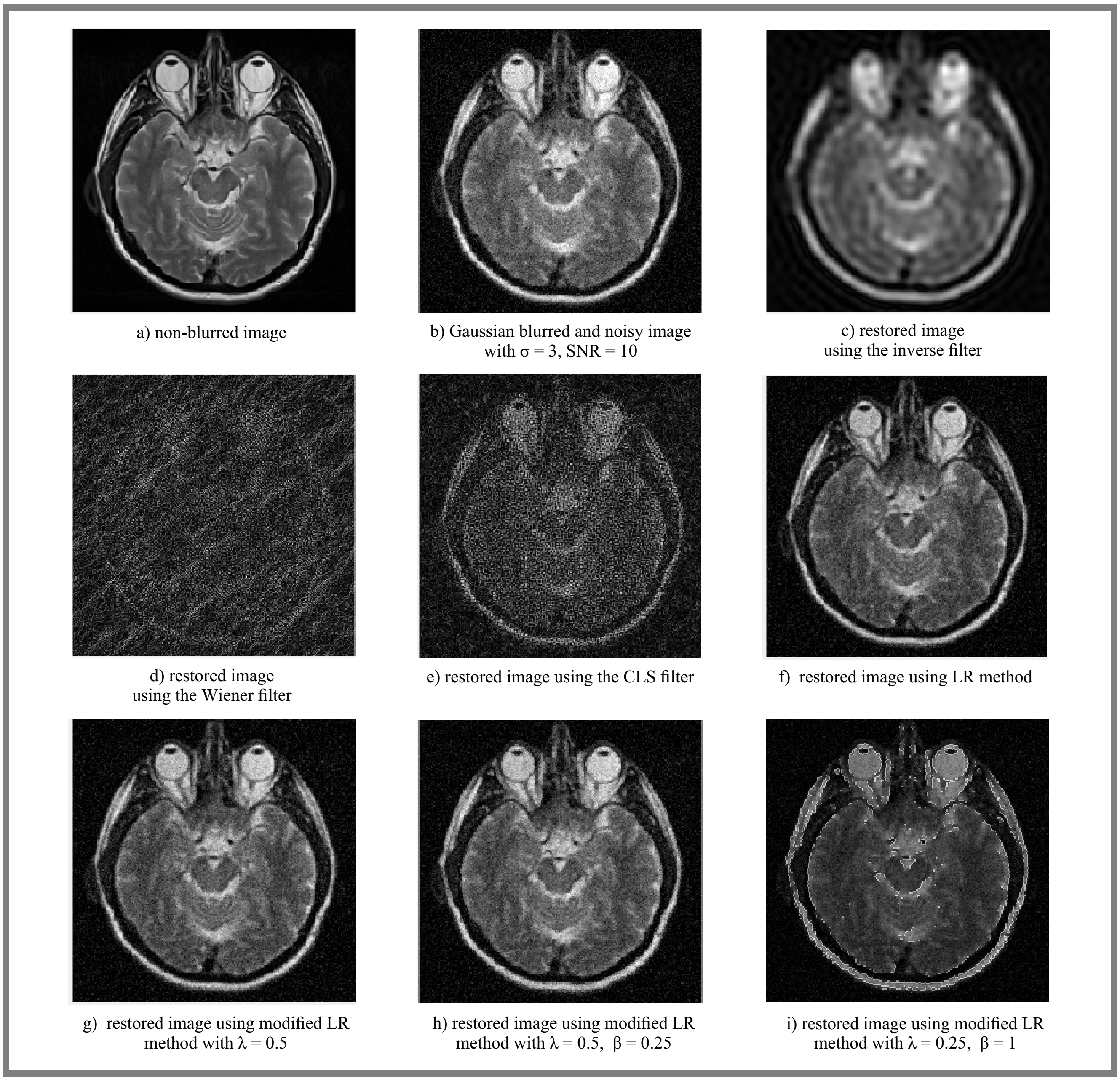
a) non-blurred image
b) Gaussian blurred and noisy image with σ = 3, SNR = 10
c) restored image using the inverse filter
d) restored image using the Wiener filter
e) restored image using the CLS filter
f) restored image using LR method
g) restored image using modified LR method with λ = 0.5
h) restored image using modified LR method with λ = 0.5, β = 0.25
i) restored image using modified LR method with λ = 0.25, β = 1

Fig. 8. Results of the restored CT scan image for σ = 1, SNR = 10.

and the degraded (blurred and noisy) image: peak signal to noise ratio (PSNR), structural similarity index (SSIM), and root mean square error (RMSE). A reference metric that requires both a reference image and a processed image to be acquired from the same image is called a full reference metric. These metrics are given by [28]:

$$\mathrm{PSNR} = 20\log\frac{\mathrm{MAX}_f}{\sqrt{\mathrm{MSE}}}\,, \tag{12}$$

where MAX_f is its highest possible pixel value, i.e. 255 for 8 bits per sample, and MSE stands for root mean square error:

$$SSIM_{(x,y)} = \frac{(2\mu_x\mu_y + C_1)(2\sigma_{XY} + C_2)}{(\mu_x^2 + \mu_y^2 + C_1)(\sigma_x^2 + \sigma_y^2 + C_2)}\,, \tag{13}$$

where: x and y are windows of similar size, μ_x, μ_y are the means of x and y, respectively, variances of x and y are σ_x^2 and σ_y^2, respectively, and covariance between x and y is denoted by σ_{XY}. To keep the stability of computation, constants C_1 and C_2 are utilized. By default: $C_1 = (k_1 l)^2$, $C_2 = (k_2 l)^2$, where l is the pixel values' dynamic range (255 for 8-bit), $k_1 = 0.01$, $k_2 = 0.03$:

$$RMSE = \sqrt{\frac{1}{MN}\sum_{x=0}^{m-1}\sum_{y=0}^{n-1}\left[f(x,y) - g(x,y)\right]^2}\,, \tag{14}$$

where: $f(x,y)$ is the original image, $g(x,y)$ is the degraded image, while N and M represent the image dimensions.

Tab. 1. RMSE of restored images with a different type of filter.

Filter type	**STD σ**	**RMSE, no noise**	**RMSE, SNR = 10**	**RMSE, SNR = 50**	**RMSE, SNR = 100**
Direct inverse filter	1	0.511	0.511	0.511	0.511
	3	0.544	0.544	0.544	0.544
Wiener filter	1	0.508	0.495	0.506	0.507
	3	0.544	0.526	0.538	0.541
Constrained least squares filter	1	0.508	0.506	0.508	0.508
	3	0.544	0.526	0.538	0.540
R-L filter	1	0.196, 2 iter.	0.263, 1 iter.	0.237, 1 iter.	0.207, 2 iter.
	3	0.269, 15 iter.	0.293, 13 iter.	0.268, 15 iter.	0.267, 15 iter.
Adaptive R-L filter $\lambda = 0.5$	1	0.195	0.263	0.217	0.206
	3	0.256	0.295	0.262	0.261
Adaptive R-L filter $\lambda = 0.5$, $\beta = 0.25$	1	0.252	0.261	0.256	0.251
	3	0.306	0.290	0.311	0.315
Adaptive R-L filter $\lambda = 0.25$, $\beta = 1$	1	0.341	0.364	0.260	0.343
	3	0.356	0.380	0.310	0.371

Tab. 2. RMSE of images restored with the R-L filter, versus iteration number.

	$\sigma = 1$ **no noise**	$\sigma = 3$ **no noise**	$\sigma = 1$ **SNR = 10**	$\sigma = 1$ **SNR = 50**	$\sigma = 1$ **SNR = 100**	$\sigma = 3$ **SNR = 10**	$\sigma = 3$ **SNR = 50**	$\sigma = 3$ **SNR = 100**
1	0.212	0.304	0.263	0.237	0.216	0.323	0.304	0.304
2	0.196	0.295	0.267	0.244	0.207	0.313	0.294	0.294
3	0.207	0.289	0.281	0.262	0.212	0.308	0.288	0.288
4	0.221	0.285	0.293	0.280	0.228	0.304	0.284	0.284
5	0.231	0.282	0.295	0.295	0.249	0.301	0.281	0.281
6	0.246	0.279	0.316	0.307	0.264	0.300	0.279	0.278
7	0.266	0.277	0.333	0.320	0.289	0.298	0.277	0.276
8	0.282	0.275	0.356	0.331	0.305	0.297	0.275	0.274
9	0.293	0.274	0.366	0.341	0.315	0.295	0.274	0.272
10	0.299	0.273	0.376	0.350	0.308	0.294	0.273	0.271
11	0.313	0.272	0.384	0.358	0.317	0.294	0.272	0.270
12	0.322	0.271	0.389	0.365	0.326	0.293	0.271	0.269
13	0.336	0.270	0.395	0.372	0.341	0.293	0.270	0.268
14	0.349	0.269	0.402	0.378	0.352	0.293	0.269	0.267
15	0.356	0.269	0.407	0.383	0.358	0.293	0.268	0.267

Table 1 shows the performance evaluation results with varying width σ of the blurring function, for different values of real widths.

The variation of RMSE in filters presented in Tab. 1 can be summarized as:

- RMSE of degraded images in (Wiener, CLSF, R-L) filters decreases with increasing SNR and increases with increasing σ of the Gaussian blurring function,
- for an inverse filter, RMSE of degraded images increases with increasing σ of the Gaussian blurring function and is unaffected by SNR variation,
- RMSE of the restored image is lower than that of the inverse filter when using (Wiener and CLSF) filters,
- the R-L filter reduces RMSE of the restored image more than Wiener and CLSF,
- RMSE of the restored image is lower than RMSE of all other filters when using an adaptive R-L with $\lambda = 0.5$,
- RMSE of the image restored using an adaptive R-L filter with $\lambda = 0.5$ and $\beta = 0.25$ is lower than the R-L filter with SNR = 10.

Tab. 3. Metrics of images restored with the adaptive R-L filter with various λ, β.

λ; β	**σ, SNR**	**σ = 1**	**σ = 3**	**σ = 1**	**σ = 1**	**σ = 3**	**σ = 3**
		no noise	**no noise**	**SNR = 10**	**SNR = 100**	**SNR = 10**	**SNR = 100**
0.25, 0	RMSE	0.19	0.25	0.26	0.20	0.29	0.25
	PSNR	28.39	23.51	23.21	27.24	21.17	23.45
	SSIM	0.89	0.76	0.48	0.76	0.47	0.66
0.5, 0	RMSE	0.19	0.25	0.26	0.20	0.29	0.26
	PSNR	28.39	23.61	23.15	27.40	21.20	23.32
	SSIM	0.89	0.77	0.49	0.76	0.46	0.66
1, 0	RMSE	0.19	0.26	0.26	0.20	0.29	0.26
	PSNR	28.51	23.20	23.25	27.35	21.24	22.85
	SSIM	0.89	0.76	0.48	0.76	0.47	0.66
0.25, 0.25	RMSE	0.25	0.30	0.28	0.25	0.32	0.30
	PSNR	23.92	20.46	21.97	23.63	19.70	20.55
	SSIM	0.86	0.70	0.43	0.71	0.38	0.60
0.5, 0.25	RMSE	0.25	0.30	0.26	0.25	0.29	0.31
	PSNR	23.91	20.54	22.01	23.97	19.51	20.01
	SSIM	0.86	0.69	0.43	0.71	0.37	0.59
1, 0.25	RMSE	0.26	0.31	0.28	0.25	0.33	0.32
	PSNR	23.76	19.96	21.80	23.81	19.08	19.76
	SSIM	0.86	0.70	0.42	0.71	0.36	0.58
0.25, 0.5	RMSE	0.19	0.26	0.28	0.20	0.32	0.31
	PSNR	22.91	20.24	21.59	23.20	19.29	20.17
	SSIM	0.83	0.69	0.44	0.70	0.37	0.60
0.5, 0.5	RMSE	0.26	0.31	0.29	0.26	0.33	0.31
	PSNR	23.37	20.20	21.28	23.33	19.25	20.00
	SSIM	0.84	0.69	10.73	0.71	0.39	0.60
1, 0.5	RMSE	0.26	0.32	0.28	0.26	0.32	0.31
	PSNR	23.40	19.73	21.79	23.14	19.40	19.90
	SSIM	0.85	0.69	0.44	0.70	0.37	0.59
0.25, 1	RMSE	0.34	0.35	0.36	0.34	0.38	0.37
	PSNR	18.67	17.93	17.53	18.56	16.79	17.20
	SSIM	0.76	0.66	0.48	0.69	0.44	0.60
0.5, 1	RMSE	0.31	0.34	0.34	0.32	0.36	0.35
	PSNR	19.83	18.72	18.51	19.71	17.43	18.0
	SSIM	0.79	0.67	0.47	0.70	0.43	0.61
1, 1	RMSE	0.28	0.32	0.31	0.29	0.34	0.33
	PSNR	21.57	19.69	20.20	21.47	18.32	19.04
	SSIM	0.81	0.68	0.49	0.72	0.43	0.60

RMSE summary for the R-L filter is shown in Tab. 2. The commentary is as follows:

- RMSE of degraded images increases along with increasing σ of the Gaussian blurring function and decreases with increasing SNR,
- the number of iterations increases with increasing the degradation parameters.

The restoration iteration is achieved when no change may be detected between the current restored image and the previous one. In such a situation, the repetition process is terminated.

5. Conclusion and Future Work

The results from simulation show that when using a small value of parameters λ and β, the adaptive R-L filter performs better in image quality restoration, as the Gaussian blurring function's standard deviation values and SNR increase with each iteration. The experimental results show a decrease in the RMSE value of up to 0.25 when using $\lambda = 0.5$ in one iteration, compared to other existing methods, for example the Wiener filter, where RMSE values reach 0.5442. This demonstrates the effectiveness of our proposal in terms of improved accuracy of the medical image by adapting the R-L algorithm, but the results were not satisfactory when using large values of the parameters λ and β. We will continue work to improve the accuracy of the solution and to solve that problem in the future. It is also possible to use another type of the point spread function (PSF) and noise that can be applied in conjunction with the proposed framework in the near future.

References

[1] P. Gupta and R. Mehra, "Blind restoration method for satellite images using memetic algorithm", *International Journal of Computer Applications*, vol. 130, no. 1, pp. 20–25, 2015 (https://doi.org/10.5120/ijca2015906857).

[2] R. Mishra, N. Mittal, and S.K. Khatri, "Digital image restoration using image filtering techniques", *International Conference on Automation, Computational and Technology Management* (*ICACTM*), London, UK, 2019, (https://doi.org/10.1109/ICACTM.2019.8776813).

[3] P. Ganesan and V Rajini, "Comparative study of denoising methods for satellite image restoration using Matlab", *International Journal of Advanced Research in Computer Science*, vol. 5, no. 4, pp. 74–77, 2013 (http://www.ijarcs.info/index.php/Ijarcs/article/view/1685/1673).

[4] M.K. Kadhom, A.A. Al-Ani, and S.A. Saleh, "Image restoration using adaptive nonlinear techniques", M.Sc. thesis, Al-Nahrain University, Baghdad, Iraq, 2008.

[5] M.A. Kadhim, Ed., "Restoration medical images from speckle noise using multifilters", *7th International Conference on Advanced Computing and Communication Systems* (*ICACCS*), Coimbatore, India, 2021 (https://doi.org/10.1109/ICACCS51430.2021.9441814).

[6] G.S. Karam, Z.M. Abood, H.H. Kareem, and H.G. Dowy, "Blurred image restoration with unknown point spread function", *Al-Mustansiriyah Journal of Science*, vol. 29, no. 1 pp. 189–194, 2018 (https://doi.org/10.23851/mjs.v29i1.335).

[7] K. Panfilova and S. Umnyashkin, "Linear blur compensation in digital images using Lucy-Richardson method", *2016 IEEE NW Russia Young Researchers in Electrical and Electronic Engineering Conference* (*EIConRusNW*), 2016 (https://doi.org/10.1109/EIConRusNW.2016.7448179).

[8] O. Anacona-Mosquera, J. Arias-García, D.M. Muñoz, and C.H. Llanos, "Efficient hardware implementation of the Richardson-Lucy algorithm for restoring motion-blurred image on reconfigurable digital system", *29th Symposium on Integrated Circuits and Systems Design* (*SBCCI*), Belo Horizonte, Brazil, 2016 (https://doi.org/10.1109/SBCCI.2016.7724056).

[9] A. Tselousov and S. Umnyashkin, "Kernel estimate for image restoration using blind deconvolution", *2017 IEEE Conference of Russian Young Researchers in Electrical and Electronic Engineering* (*EIConRus*), St. Petersburg and Moscow, Russia, 2017 (https://doi.org/10.1109/EIConRus.2017.7910667).

[10] F. Aouinti, N. M'barek, M.M. Nasri, M. Moussaoui, and B. Bouali, "An improved Richardson-Lucy algorithm based on genetic approach for satellite image restoration", *International Arab Journal of Information Technology*, vol. 15, no. 4, 2018 (https://iajit.org/portal/PDF/July%202018,%20No.%204/11791.pdf).

[11] K. Panfilova and S. Umnyashkin, "Correlation-based quality measure for blind deconvolution restoration of blurred images based on Lucy-Richardson method", *2019 IEEE Conference of Russian Young Researchers in Electrical and Electronic Engineering* (*EIConRus*), Saint Petersburg and Moscow, Russia, 2019 (https://doi.org/10.1109/EIConRus.2019.8657324).

[12] D. Liu, X. Chen, and X. Liu, "An improved Richardson-Lucy algorithm for star image deblurring", *2019 IEEE International Instrumentation and Measurement Technology Conference* (*I2MTC*), Auckland, New Zealand, 2019 (https://doi.org/10.1109/I2MTC.2019.8826905).

[13] K. Breykina and S. Umnyashkin, "Correlation-based iterative estimation of distortion kernel for image restoration", *2020 IEEE Conference of Russian Young Researchers in Electrical and Electronic Engineering* (*EIConRus*); St. Petersburg and Moscow, Russia, 2020 (https://doi.org/10.1109/EIConRus49466.2020.9039119).

[14] B. Zhao, X. Chen, G. Feng, X. Zhao, and J. Jiang, Eds., "An improved LR algorithm for image deblurring", *2020 Chinese Control and Decision Conference* (*CCDC*), Hefei, China, 2020 (https://doi.org/10.1109/CCDC49329.2020.9164762).

[15] D. Bhonsle, "Quality improvement of Richardson Lucy Based deblurred images using krill herd optimization", *2021 International Conference on Advances in Electrical, Computing, Communication and Sustainable Technologies* (*ICAECT*), Bhilai, India, 2021 (https://doi.org/10.1109/ICAECT49130.2021.9392469).

[16] D. Lyu, J. Tian, H. Hu, and X. He, "Ultrasonic c-scan image restoration method using the Richardson-Lucy algorithm and a flaw measurement model", *Applied Acoustics*, vol. 200, 109074, 2022 (https://doi.org/10.1016/j.apacoust.2022.109074).

[17] Y. Li *et al.*, "Incorporating the image formation process into deep learning improves network performance", *Nature Methods*, vol. 19, pp. 1427–1437, 2022 (https://doi.org/10.1038/s41592-022-01652-7).

[18] H. Joshi and D.J. Sheetlani, "Image restoration techniques in image processing: An illustrative review", *International Journal of Advance Research in Science and Engineering*, vol. 6, no. 1, pp. 145–158, 2017 (http://www.ijarse.com/images/fullpdf/1512719410_1023_IJARSE.pdf).

[19] N.K. El Abbadi, A.H. Abdulkhaleq, and S.A. Al Hassani, "A survey on blind de-blurring of digital image", *Iraqi Journal of Science*, vol. 63, no. 1, pp. 338–352, 2022 (https://doi.org/10.24996/ijs.2022.63.1.32).

[20] D. Fish, A. Brinicombe, E. Pike, and J. Walker, "Blind deconvolution by means of the Richardson-Lucy algorithm", *Journal of the Optical Society of America A*, vol. 12, no. 1, pp. 58–65, 1995 (https://doi.org/10.1364/JOSAA.12.000058).

[21] R.S.H. Al-Taweel and H.G. Daway, "Deblurring average blur by using adaptive Lucy Richardson", *Journal of College of Education*, no. 5, pp. 75–90, 2015 (https://www.iasj.net/iasj/download/dd42a7cdacecf1d6).

[22] M. Juneja and P.S. Sandhu, "Performance evaluation of edge detection techniques for images in spatial domain", *International Journal of Computer Theory and Engineering*, vol. 5, no. 1, pp. 614–621, 2009 (https://doi.org/10.7763/IJCTE.2009.V1.100).

[23] T. Sanida, A. Sideris, and M. Dasygenis, Eds., "A heterogeneous implementation of the Sobel edge detection filter using OpenCL", *2020 9th International Conference on Modern Circuits and Systems Technologies* (*MOCAST*), Bremen, Germany, 2020 (https://doi.org/10.1109/MOCAST49295.2020.9200249).

[24] A.H. Muhammad and H.S. Akbar, "Algorithms for edge detection by using fuzzy logic technique", *Kirkuk University Journal-Scientific Studies*, vol. 10, no. 1, pp. 173–190, 2015 (https://doi.org/10.32894/kujss.2015.101966).

[25] C. Saravanan, "Color image to grayscale image conversion", *2010 Second International Conference on Computer Engineering and Applications*, Bali, Indonesia, 2010 (https://doi.org/10.1109/ICCEA.2010.192).

[26] S. Patro and K.K. Sahu, "Normalization: A preprocessing stage", *International Advanced Research Journal in Science, Engineering and Technology*, vol. 2, no. 3, pp. 20–22, 2015 (https://doi.org/10.17148/IARJSET.2015.2305).

[27] M.H. Muhsonand A.A. Al-Ani, "Blind restoration using convolution neural network", *Iraqi Journal of Information and Communication Technology*, vol. 1, no. 1, pp. 25–32, 2021 (https://doi.org/10.31987/ijict.1.1.178).

[28] M.A. Abdulrahman and A.H. Al-Fayadh, "Modifications with applications of some transforms in image processing", M.Sc. thesis, Al-Nahrain University, Baghdad, Iraq, 2018.

Qunoot A. Yaqoub
M.Sc. student at the Department of Information and Communication Engineering
E-mail: mohqunoot@gmail.com
College of Information Engineering, Al-Nahrain University, Baghdad, Iraq

Ayad A. Al-Ani, Prof.
Professor of Digital Image Processing at the Department of Information and Communication Engineering
E-mail: ayad.a@nahrainuniv.edu.iq
College of Information Engineering, Al-Nahrain University, Baghdad, Iraq